

Application of Dynamic Mode Decomposition for Improved Optics Measurements from s^* Movement at sPHENIX

William Fung and Yue Hao

Department of Physics and Astronomy, Michigan State University, East Lansing, MI 48824, USA

Xiaofeng Gu and Guillaume Robert-Demolaize

Brookhaven National Laboratory, Upton, NY 11973, USA

(Dated: March 17, 2025)

Current average horizontal beta beat measurements between operating Interaction Regions (IR) at the Relativistic Heavy Ion Collider (RHIC) are around 15% along with significant variation in s^* . This threshold to measure the linear optics can be improved by considering decomposition techniques involving data reconstruction such as Dynamic Mode Decomposition (DMD) on turn-by-turn (TBT) datasets, along with cross-checking between different method variations. These were then applied to analyze the movement of s_x^* at the 8 o'clock IR at RHIC (IR8). This movement was done using a sensitivity matrix to determine magnet strengths necessary to move s_x^* without disturbing other optics. Decomposition techniques were found to significantly aid in beat reduction around IP, with DMD demonstrating the least variability between decomposition techniques and between s_x^* movements. These decomposition techniques will be implemented into RHIC for future linear optics analysis.

I. INTRODUCTION

The luminosity is vital in delivering high quality physics experiments at STAR and sPHENIX, located at IR6 and IR8 of the RHIC ring, respectively. The optics near each IR must be accurately controlled so that both colliding beams reaches its desired beam size at designed longitudinal position with respect to the detector location. We characterized the IR optics by the minimum of the beta function (β^*) located at s^* at each IR [1]. Therefore, precise measurements and adjustment of optics, especially of transverse s^* , is crucial to ensure maximal luminosity output.

Methods to measure the beta function and to minimize the difference between measurement and model (beta beat) have been developing throughout the history of synchrotron research with the utilization of beam position monitor (BPM) data. Methods such as Fourier analysis, N-bpm method, and phase advance methods [2, 3] take advantage of TBT data from bpms to calculate linear optics through phase and tune. Another class traditionally developed by lepton storage rings calculates the orbit response matrix (ORM) built from observing orbit responses from corrector kicks. The Linear Optics for Closed Orbit (LOCO) method utilizes this matrix to optimally correct the magnet strengths using a model and minimize the beta beat [4]. While accurate, the ORM methods can usually take hours depending on the quality of the correctors. On the other hand, TBT methods are quick but are prone to limited, less accurate BPM measurements depending on the BPM quality. SPEAR3 has shown that these two methods could be combined for a fast and accurate model from simulation [5].

The current optics correction algorithm at RHIC measures the beta function by fitting a curve to the closed orbit oscillations with decoherence. The final decoherence model from [6] is simplified such that the least amount of

parameters were used while retaining the general structure of the data, given by Eq. (1). The TBT signal is modeled by amplitude a , the decoherence coefficient b , the machine tune ν , and the phase offset d . Therefore, only a few turns are necessary and the generality takes care of noise and other BPM errors when measuring linear optics. A simplified model also optimizes the computational processing since calculations were done for every bpm. The average transverse beta beat around RHIC using this method is about 10% percent as shown in Fig. 1.

$$x_{co} = a \exp(bn) \cos(2\pi\nu n + d) \quad (1)$$

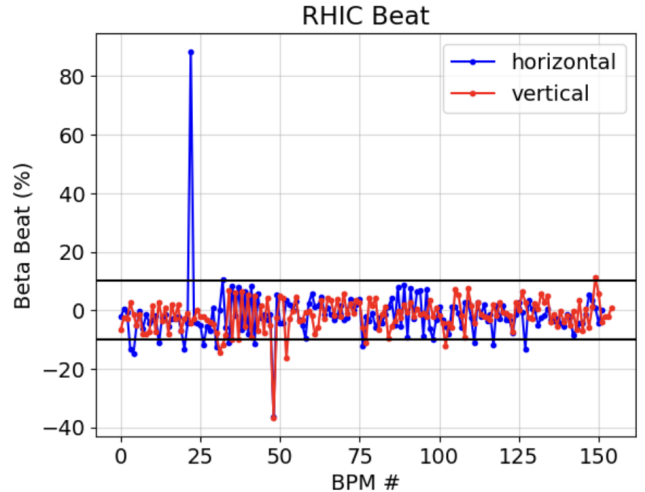


FIG. 1. Measured horizontal (blue) and vertical (red) beta beat from curve fit method vs BPM number. The solid black lines indicate beta beat $\pm 10\%$

However, when TBT data is repeatedly taken during

an experiment, linear optics measurements are inconsistent. While the average beta beat remains fairly consistent, the average beta beat around IR, especially at IR8, suffers due to larger amplitudes from corresponding BPMs, making TBT data more sensitive to BPM errors. This is highlighted when measuring the average beta beat near the interaction point (IP6 & 8) in Fig. 2. While the vertical beta beat remains low, the horizontal has been estimated to be around 15%. The resulting transverse s^* measurements are also close to zero on average. However, both beta beat and s^* at IP8 show high variance in data, leading to inconsistent measurements of the optics, even when s^* has not been moved ($\Delta s^* = 0$). Since the sPHENIX detector has a vertex detection within ± 10 cm [7], more accurate and consistent s^* measurements and adjustments will greatly aid luminosity maximization.

The previous method mentioned also involves calculations from a model such as MADX (Methodical Accelerator Design) to determine the beta function. MADX can be used to model accelerators by element and thus calculate optics functions in an ideal system. The amplitude from Eq. (1) is used along with MADX to calculate the action. This factor is then used to scale the amplitude function into a measurement of the beta function. Since the action is calculated using MADX, this can cause bias towards the model, as these methods could unintentionally skew the results to match the model's beta function.

Alternatively, if two BPMs are separated by a well informed lattice, e.g. a drift space, we can retrieve the optics function on these BPMs using a model-independent approach. For a pair of BPMs separate by drift space, e.g. the BPMs on either side of detector when the detector solenoid is not turned on, this method take advantages of calculable angle coordinates x' from the BPM readings. The transfer matrix of transverse phase space could then be built using linear regression (LR analysis) and the beta function, β^* , and s^* can be calculated accordingly. This gets rid of the need for the model in the calculation since the intermediate amplitude function is not present. Combined with various decomposition techniques that generalize the data before analysis, these methods are expected to increase the accuracy and consistency of the linear optics at IP. After the linear optics measurements are improved, the movement of s^* can then be accurately assessed.

In addition to the accuracy and consistency of β and s^* measurements, the accuracy of s^* movements to bring the beam to the minimum location is also critical to luminosity maximization, especially when crossing angle and short bunch length are planned for optimizing the vertex luminosity for SPHENIX experiment. Moving s^* is usually done by optics tuning, or varying magnet strengths of insertion quadrupoles near IRs. This is previously achieved by RHIC through MADX matching algorithms using the RHIC lattice model. However, this has led to an inaccurate assessment of s^* locations and ultimately inaccurate β^* measurements. An alternative method using the sensitivity matrix was attempted in this experiment.

This paper is structured in accordance with the following experimental procedure for the adjustments and measurement at beta waist locations. First, we introduce the proposed algorithm for adjusting s^* in Section II, using an example where s_x^* at IP8 is modified. The calculation of the required magnet strengths is then performed via a sensitivity matrix. These values are then sent to RHIC and TBT measurements are taken followed by exciting the betatron motion by the kicker during the accelerator experiments at RHIC. Next, the resulting TBT data is preprocessed using methods described in Section III. The preprocessed data is subsequently analyzed using LR methods described in Section IV to get measured values of s^* at IP8 as well as other optical functions. Finally, results and comparisons between different optics measurement methods and various modal decomposition techniques are discussed in Section V.

II. OPTICS TUNING

To achieve better control of the IR lattice, an approach using the sensitivity matrix B [8] was utilized, where B represents an approximately linear relationship between the change in magnet strengths ΔK and change in optics ΔO . However, the current changes ΔI were used in place of ΔK due to the nonlinear relationship between K and I . This relation between ΔI and ΔO is reflected in Eq. (2). These power supply values were then converted to magnet strengths when sent to RHIC.

$$\Delta O = B \Delta I \quad (2)$$

I consists of seventeen power supply currents that affect the insertion quadrupoles within IR8. O includes thirteen optics: transverse s^* , β^* , and horizontal dispersion at IP; and optics at the upstream end of IR8 (between insertion and arc regions): transverse β , α , μ , horizontal dispersion, and change in horizontal dispersion. These are equivalent to the matching method; minimal changes to these optics results in minimal changes in optics throughout the ring.

To calculate B , ΔI was varied by ± 1 Amp and the resulting ΔO was calculated using MADX. A linear regression was then performed to compute B . A correlation coefficient close to one was measured, demonstrating linearity within ± 1 Amp.

As we will demonstrate in the experiment, to move s_x^* while keeping the other optical quantities constant, the currents required can be calculated from the pseudo-inverse of B from Eq. (3). This can be extended to moving s_y^* or any other optical quantities in IR while maintaining certain constraints.

$$\Delta I_0 = B^{-1} \begin{bmatrix} s_x^* \\ 0 \\ \vdots \\ 0 \end{bmatrix} \quad (3)$$

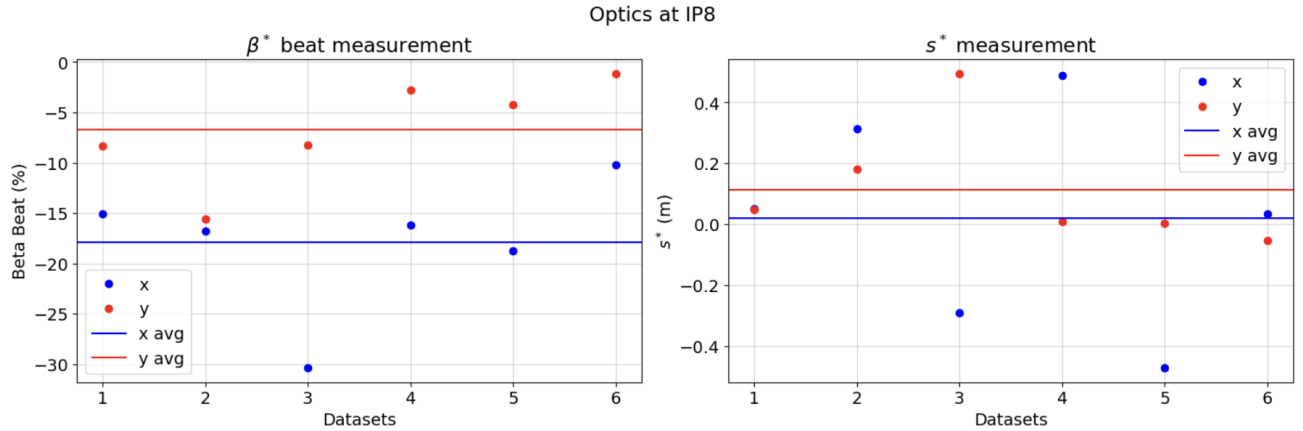


FIG. 2. Measured horizontal (blue) and vertical (red) beta beat and s^* measurements at IP8 vs BPM number on the left and right respectively. Six TBT datasets with no movement of s^* ($\Delta s^* = 0$) were analyzed.

The power supply limits as well as hysteresis effects from quadrupoles were taken into account by optimizing the current, magnet strengths, and optics. This was done using the null space of B using (4), as Eq. (2) is an under-determined system.

$$\Delta I_C = B^{-1} \begin{bmatrix} s_x^* \\ 0 \\ \dots \\ 0 \end{bmatrix} - \text{Null}(B)C \quad (4)$$

Where C is a vector of constants whose size is the number of free parameters in the system (in this case, four). These are chosen such that the power supply limits, current jumps, hysteresis effects, and other added constraints are respected in Table I. The null space accesses the infinite solutions near I_0 such that the optics requirements are unchanged:

$$B\Delta I_C = B\Delta I_0$$

This optimization method also has the advantage of applying other constraints to mitigate beam losses. The beta function at collimators near IR8 were made sure to be below the original value to reduce risk of beam loss and collimator damage shown in Table I. However, there is no guarantee that a solution can be found for a given optics movement depending on the initial lattice and the constraints employed, and one may have to relax the constraints or move to a nonlinear method with a well-defined inverse.

Each movement of s_x^* produces the resulting current values, optics, and magnet strengths. The current values are inspected to confirm no current limits were violated; all other values were inspected to confirm optimization, correctness, and accuracy. We have demonstrated that solutions can be found in range of ± 0.5 meters for the proton-proton lattice and are sufficient for our purpose of sPHENIX collision point optimization. The resulting

magnet strengths are then stored in trim files for each movement of s_x^* and sent to machine during experiment. The magnet strengths used in the experiment are shown in Table II.

III. PREPROCESSING

The optics functions are determined from the TBT data after the beam is kicked by a corrector (ARTUS) [3] around IR6. The TBT data from RHIC yields average positions for 1024 turns in 168 and 167 horizontal and vertical BPMs respectively. Fig. 3 is a visual example of the first BPM. Preprocessing this data is crucial as it prepares the data for the upcoming optics measurement methods. Initial data analysis (IDA) improves their computational efficiency while modal decomposition techniques improve their accuracy and consistency.

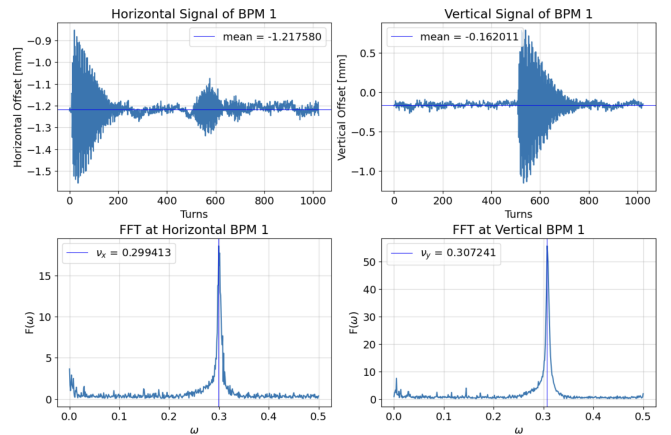


FIG. 3. TBT data (top) and respective Fourier transforms (bottom) for the first bpm. Left and right columns shows horizontal and vertical axis respectively.

TABLE I. Optics constraints to optimize the magnet solutions

Constraint	Definition	Notes
Power Supply Limits	$I_j^{lower} \leq I_j \leq I_j^{upper}$	$j \in N_{magnets}$
Change in Current Strengths	$\min(\Delta I_j)$	$j \in N_{magnets}$
Hysteresis	$\ K_j^i\ \leq \ K_j^{i+1}\ $	$i \in N_{iterations} \wedge j \in N_{magnets}$
Collimator at IR8	$\beta_u^i \leq \beta_u^0$	$i \in N_{iterations} \wedge u \in \{x, y\}$

TABLE II. Current strength solutions [A] within IR8 to move Δs^* [m]

Name	-0.5	-0.3	-0.1	0.1	0.3	0.5
psiq1-ir8	163.45703139	158.02570281	149.75102506	141.0262088	136.46518361	130.71833274
psiq2-ir8	66.09781786	59.81695935	51.60971675	44.05161838	40.11055009	35.55529409
psiq3-ir8	-224.58487004	-218.88727368	-211.07329926	-206.20288056	-206.61598533	-207.21104246
psiqt4-ir8	10.57993234	3.90198567	-4.73179012	-10.26278655	-10.26278654	-10.26278626
psiqt5-ir8	-29.5090292	-26.15845175	-22.06604234	-19.21901745	-18.53740379	-17.86996118
psiqt6-ir8	18.55534084	16.20894918	13.42448533	11.59463061	11.32927389	11.05034511
psoql1-ir8	102.75497757	97.34295801	92.60908206	83.71662111	68.71506673	54.19732412
psoql2-ir8	35.80395826	31.81267031	28.02999144	22.56156272	14.60177973	6.90666317
psoql3-ir8	-210.00944024	-209.4427006	-208.08624856	-208.07894446	-209.38575847	-211.42025927
psoqt4-ir8	-3.48207911	-0.66665457	2.3396558	3.02787834	0.88178863	-1.35543695
psoqt5-ir8	13.2903151	12.44586107	11.57425892	11.630614	12.79664592	13.99505962
psoqt6-ir8	-4.43283173	-4.02060907	-3.60825392	-3.67703198	-4.28583738	-4.92747709
psq456-ir8	83.09959578	82.53289345	81.17644144	82.57832994	86.80070581	91.57039389
psq7-ir8	81.94970651	81.94966919	81.94966916	81.7786326	81.77853103	81.77854658
psqad-ir8	75.58828199	91.37484151	105.48863718	114.68765068	119.97554057	125.20617937
psqfa-ir8	-123.27610483	-134.34569334	-144.1181543	-148.77107239	-148.77107234	-148.77107239
psqfb-ir8	-47.65333479	-66.33156114	-83.67287823	-99.72761374	-115.67436055	-131.63989502

A. Initial Data Analysis

There are certain occasions when the average beam orbit position around RHIC is displaced from the standard trajectory shown in Fig. 4 due to various orbit corrections. Centering the data shifts the focus from beam trajectory to relative average beam position from closed orbit when analyzing the data. Since these were taken at the height of the kick in Fig. 5, these variations represent the strength of the kick felt by the beam at each bpm, demonstrating that the highest felt kicks occur around IPs.

The kick from the corrector produces betatron oscillations which decay after less than 500 turns due to decoherence effects. From Fig. 3, the beam is kicked in the horizontal followed by the vertical plane to avoid coupling effects in either direction. Therefore, the data is further truncated to around 200 turns, only keeping the betatron oscillations subject to decoherence, shown in Fig. 6. This increases computation efficiency and reduces the effects of coupling in each direction.

A bad BPM refers to those whose tune does not match closely to RHIC's working point. They are zeroed out during this study to maintain quality throughout the dataset and improve the quality for model decomposition methods. A tune offset greater than 0.005 from the working point was chosen to indicate a bad bpm, shown in Fig. 7.

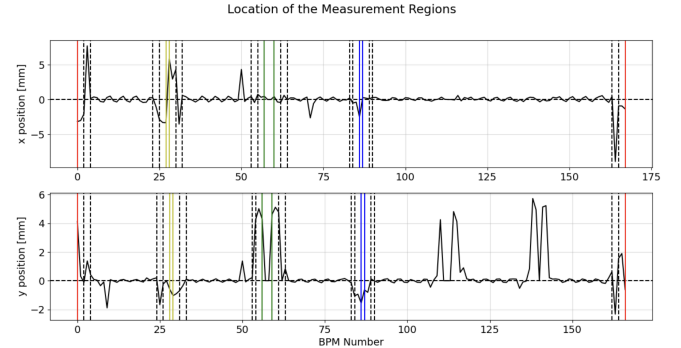


FIG. 4. Average horizontal (top) and vertical (bottom) position in mm vs bpm number after the beam has been kicked. Dotted lines show locations of drift spaces, colored regions show IRs (red: IPR6; yellow: IPR8; green: IPR10; blue: IPR12).

B. Modal Decomposition and Reconstruction

1. Principal Component Analysis

Principal Component Analysis (PCA) finds a linear transformation of the dataset to uncover the maximum amount of variance in the least number of orthogonal principal components (PC). Various data driven methods such as those in machine learning utilize PCA for dimensionality and noise reduction of large, multivariate

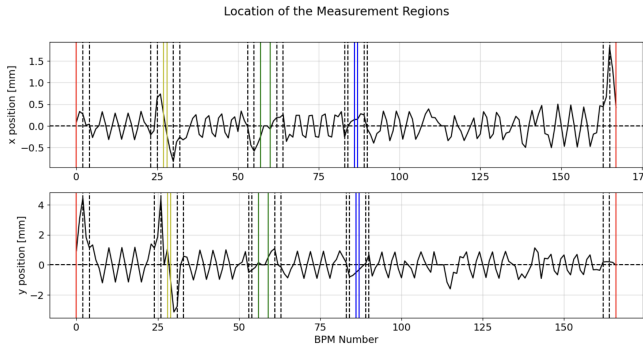


FIG. 5. Beam orbit after centering, with same axis and turn number as Fig. 4.

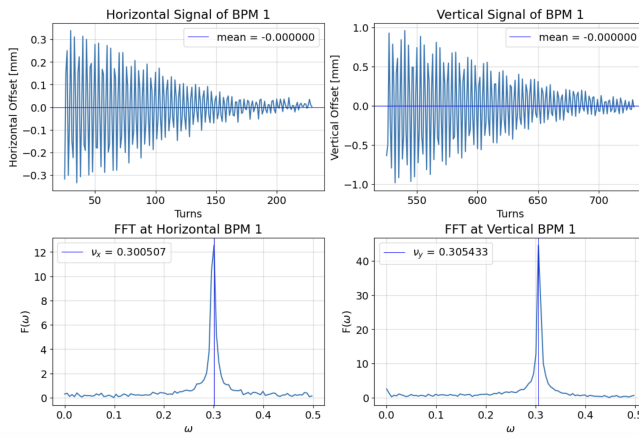


FIG. 6. Fig. 3 after truncation such that the data keeps kick and decoherence. Data yet to be centered.

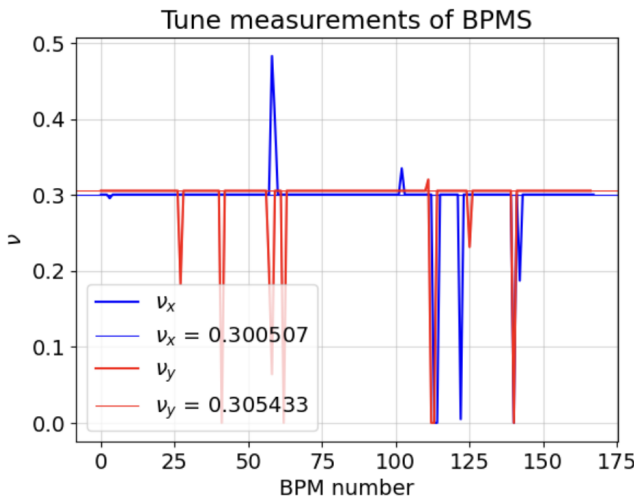


FIG. 7. Horizontal (blue) and vertical (red) tune measurements versus BPM number. Outlier BPMs are considered "bad".

datasets. The conventional way to find PCs efficiently is to use Singular Value Decomposition (SVD), where a dataset X is split into three matrices demonstrated in Eq. (5).

$$X = U\Sigma V^T \quad (5)$$

U and V are orthogonal matrices, where the rows of U represents the higher dimensional modes while the columns of V represents the low dimensional modes. Σ is a diagonal matrix of singular values, ordered by value. The largest (first) singular value corresponds to the PC that best represents the data. These values can be plotted on a scree plot, and the values before the inflection point n_s are retained when reconstructing the data shown in Eq. (6).

$$X_{PCA} = U[n_s]\Sigma[n_s]V[n_s]^T \quad (6)$$

For horizontal BPM data, PCA would create 168 orthogonal modes from a 168-dimensional space. The first four modes were chosen, and an example reconstructed plot is shown in figure Fig. 8, demonstrating cleaner data when compared to Fig. 6.

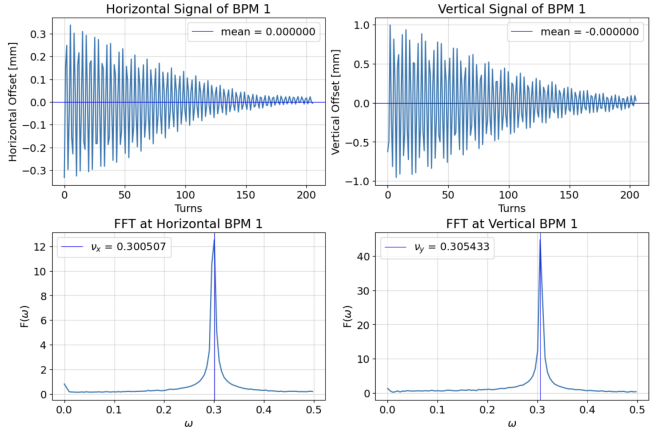


FIG. 8. Reconstructed TBT data and respective Fourier transforms after PCA for the first bpm.

2. Independent Component Analysis

One way that PCA can fall short is if independent signal modes are strongly coupled to each other. Then the orthogonal modes from PCA would be affected from each signal mode and create inaccurate ones. This was shown to be the case at the Fermilab Booster [9]. Independent Component Analysis (ICA) is usually intended to address this problem by finding independent modes rather than orthogonal ones. This method is usually used in blind source separation, where the multivariate signal is

decomposed into its source signals s . The definition of independence is given in Eq. (7)

$$\langle s_i s_j \rangle = \langle s_i \rangle \langle s_j \rangle \quad (7)$$

for two signals s_i and s_j , where $\langle \dots \rangle$ is the expected value.

Aside from the preprocessing in Section III A, ICA involves an additional preprocessing step through a process called "whitening", a technique to normalize the dataset using SVD. ICA also assumes that the source signals are also non-gaussian, which for TBT data is usually the case.

The methods in [9] involve using unequal time correlations and approximate joint diagonalization. The ICA method used in this study involves the FastICA algorithm [10] due to maturity and optimization. The algorithm initializes random signal vectors and finds the ones that describe the data by minimizing non-gaussianity while satisfying Eq. (7). This will result in a relationship between the original dataset X and the signal vectors s , related by the mixing matrix A shown in Eq. (8)

$$X = As \quad (8)$$

The first two modes are used to reconstruct the dataset since they represent the modes that make up the betatron oscillations [9]. From PCA, it was assumed that the orthogonal modes were similar to the signal modes, which might not be the case. Therefore, four modes were chosen to account for the difference, which is also where the inflection occurred. In the case of ICA, the order of the independent components as well as their respective variances cannot be determined. Therefore, the modes were selected based on how close their Fourier transforms were to the tune of the original dataset.

Since initialization of signal vectors is random, a Monte Carlo simulation was also ran and an average over reconstructed TBT data was taken. The TBT data was reconstructed using methods from [9]:

$$X_{ICA} = A_{b1}s_1 + A_{b2}s_2 \quad (9)$$

Using this method, Fig. 9 shows an example of the reconstruction of the TBT data using ICA. The TBT data still has some semblance of noise at later turns when compared to Fig. 6, but that is only due to the nature of Monte Carlo. One could find the beta function from the subsequent equations in [9], but this ultimately results in another model-dependent method. ICA will only be used as a preprocessing step in this study.

3. Dynamic Mode Decomposition

Dynamic Mode Decomposition (DMD) decomposes a time-dependent dataset into its spacial and temporal

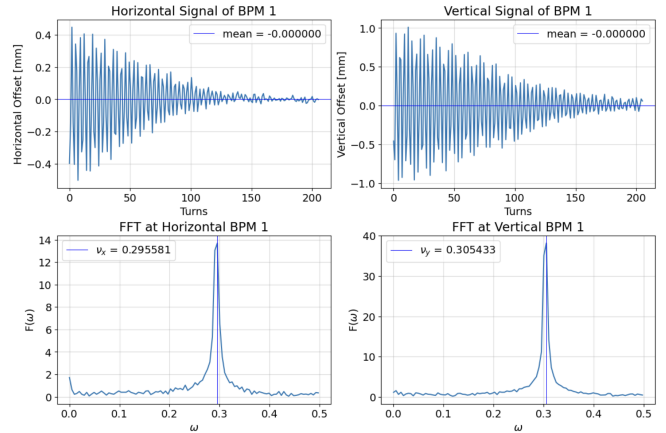


FIG. 9. Reconstructed TBT data and respective Fourier transforms after ICA for the first bpm.

modes. This method has applications in time-series forecasting in fields such as fluid dynamics. It has also been proven to be closely related to the Koopman operator, making it applicable to nonlinear systems [11].

The Exact DMD algorithm was used in this paper. Let X_i be the original dataset with 0 to $N_t - 1$ time steps, and let X_{i+1} be the dataset with 1 to N_t time steps and N_s spacial values. Then a linear relationship advance shown in Eq. (7) advances X_i one time step into the future X_{i+1} , related by some matrix D .

$$X_{i+1} = DX_i \quad (10)$$

D can be solved for by taking the psuedo-inverse of X_{i+1} and multiplying by X_i . For most datasets, this is infeasible since the size of X_{i+1} is large ($N_t N_s$) to compute psuedo-inverse, and the resulting size of D (N_s^2) is also large to compute eigen-decomposition. To solve this, a new matrix \tilde{D} is built from the SVD of both X_i and X_{i+1} . Retaining $n_s < N_s$ singular values reduces the size of D to $|\tilde{D}| = n_s^2$. The eigen-decomposition of \tilde{D} is calculated since it has been proven that the eigen-decompositions of D and \tilde{D} are identical [11].

\tilde{D} can be decomposed into spacial modes (eigenvectors Φ) and corresponding temporal modes (eigenvalues Λ). The reconstruction of the dataset is then the combination of these eigenmodes shown in Eq. (11) [12], where x_1 represents initial conditions of the system (turn t_0), and X_{DMD} predicts the turns after $t > t_0$.

$$x_1 = \Phi z \quad (11a)$$

$$X_{DMD} = \Phi \exp\left(\frac{\log(\Lambda)t}{\Delta t}\right) z \quad (11b)$$

A python library (pyDMD) was used to calculate Exact DMD (DMD) directly [13]. Utilizing this, DMD aids in creating a dataset with minimal noise shown in Fig. 10, similar to X_{PCA} and X_{ICA} .

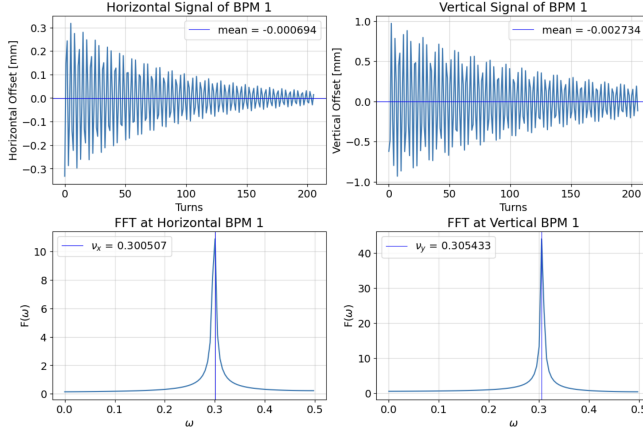


FIG. 10. Reconstructed TBT data and respective Fourier transforms after DMD for the first bpm.

IV. LINEAR OPTICS MEASUREMENT

After the TBT data has been preprocessed through centering, truncation, removal of bad bpms, and with one of the modal decomposition methods, it is now prepared to be analyzed for linear optics.

A. Phase Transfer Matrix

The phase transfer matrix (or one-turn map for rings) can be constructed along drift spaces since the angle coordinate can only be calculated at these locations [14]. RHIC currently has twelve operating drift space regions that can be used for LR analysis: four IR regions, four downstream, and four upstream of each IR. Regions that are not IRs are between the "3" and "4" magnets (bobb3/b4 for the blue ring) upstream and downstream. At each of the drift spaces, the angle coordinate u'_{12} can be calculated between the start and end points u_1 and u_2 of the drift space (downstream and upstream bpms) through Eq. (12).

$$u'_{12} = \frac{u_2 - u_1}{L} \quad (12)$$

Where L is the length of the drift space. u represents the horizontal or vertical axis. The equation for the phase transfer matrix is of the form:

$$\tilde{U} = M_j U \quad (13)$$

where:

$$U = U_j^i = \begin{bmatrix} u \\ u' \end{bmatrix}_j^i \quad (14a)$$

$$\tilde{U} = X_j^{i+1} = \begin{bmatrix} u \\ u' \end{bmatrix}_j^{i+1} \quad (14b)$$

contains information of the dataset in the horizontal or vertical axis at the drift space for the i^{th} turn and the j^{th} bpm, and

$$M_j = \begin{bmatrix} \cos \phi + \alpha \sin \phi & \beta \sin \phi \\ -\gamma \sin \phi & \cos \phi - \alpha \sin \phi \end{bmatrix}_j \quad (15)$$

is the phase transfer matrix at the j^{th} bpm [14].

Since this is a linear equation (without an intercept since the data has been centered), a linear regression method was used to calculate the components of M at each drift space. The linear optics (ϕ, α, β) can then be computed using the components of the phase transfer matrix:

$$\phi = \cos^{-1} \left(\frac{M_{11} + M_{22}}{2} \right) \quad (16a)$$

$$\beta = \frac{M_{12}}{\sin \phi} \quad (16b)$$

$$\alpha = \frac{M_{11} - M_{22}}{2 \sin \phi} \quad (16c)$$

The LR method is analogous to BPM averaging methods done by [14, 15], another model-independent method. Since the equations from both methods are derived from the phase transfer matrix, both methods produce equivalent results.

B. Exponential Removal

One preprocessing method that can also be done before linear regression is to remove the exponential term from the TBT data. This is done with a curve fitting method inspired from the previously mentioned method from BNL [6]. Once the orbit has been fit, the exponential term is taken out and a modified version of x_{co} is used:

$$x_{co} = a \cos(2\pi\nu n + d) \quad (17)$$

An example of this can be seen in Fig. 11. Doing this further generalizes the beam motion, reducing complications with nonlinear and chromatic effects. It also further reduces the noise from the system in tandem with the other decomposition techniques.

This has the added benefit of more clearly visualizing the phase space without decoherence at drift spaces. After the LR analysis has been done, the phase space data can be normalized using the following transformations [14]:

$$u_{norm} = \frac{u}{\sqrt{\beta}} \quad (18a)$$

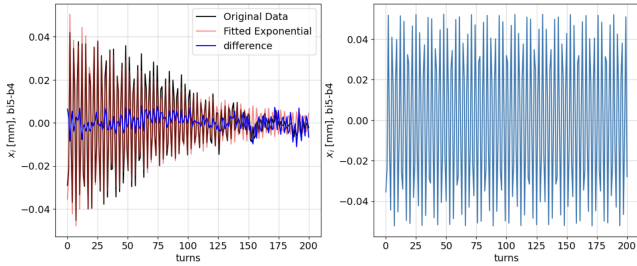


FIG. 11. The left plot shows the horizontal TBT data from the bi5-b4 BPM being fitted (orange) to the original dataset (black), and the blue shows the difference between them. The right shows the fitted curve without the exponential term from Eq. 17

$$u'_{norm} = \frac{u\alpha}{\sqrt{\beta}} + u'\sqrt{\beta} \quad (18b)$$

This is useful as a quality check to see if beam dynamics and linear optics is consistent with theory. The difference between linear optics (beta beat if α is small) can be visualized if the renormalized phase space with model linear optics are also plotted against the renormalized phase space with optics found from linear regression; The closer the two match, the smaller the difference between linear optics.

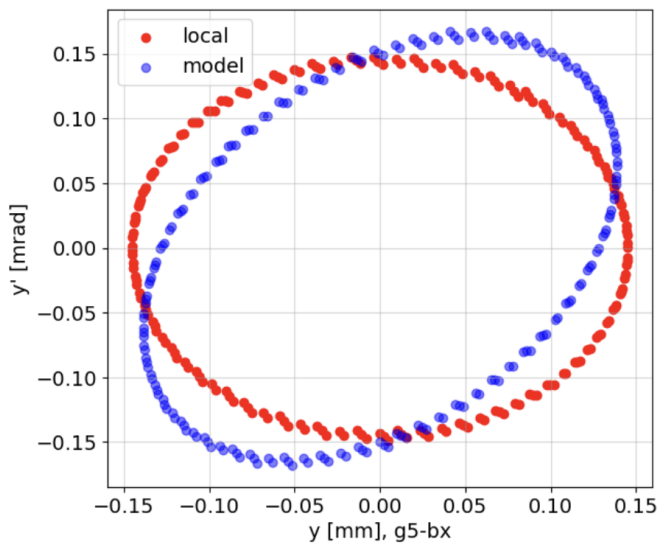


FIG. 12. The vertical phase space at the g5-bx BPM for the first 200 turns is shown. The red curve shows the phase space renormalization using linear optics measurements, and the blue curve for linear optics from model.

An example is shown in Fig. 12. Calculating the phase space in this manner will always show the measured result to be circular since the measured result is based off of the TBT data and not MADX. Nevertheless, one can see how close the measured linear optics are to the model's.

C. Linear Optics at IP

The resulting linear optics also depends on the starting turn number and the size of the interval used in LR analysis, similar to other TBT methods. This can also contribute in the ambiguity of beta function measurements. Therefore, two approaches were used during analysis: varying the interval size and varying the initial turn while keeping the respective variable constant. When varying the interval size, the interval was varied from 50 to 200 turns (average turn number for decoherence), starting from turn 0. When varying the initial turn, the initial turn was varied from 0 to 90th turn, and an interval size of 100 was used.

The average of the linear optics from these two approaches on upstream and downstream BPMs were then compared and used to determine β^* and s^* using Eq. (19). These were derived for α and β downstream of the IR from the beta function at IR in Eq. (20) [14].

$$\beta^* = \frac{\beta_1}{\alpha_1^2 + 1} \quad (19a)$$

$$s^* = s_{IP} + \alpha_1 \beta^* \quad (19b)$$

$$\beta_{IR}(s) = \beta^* + \frac{(s - s^*)^2}{\beta^*} \quad (20)$$

Fitting a curve to β and s values from the downstream and upstream bpms onto Eq. (20) would yield equivalent values of β^* and s^* . The MADX values of β^* and s^* were also calculated using this method to be compared to experimental measurements of β^* and s^* .

V. EXPERIMENTAL RESULTS

The lattice for this study consists of 12 proton bunches that were injected after ramping the blue ring at RHIC. After the beams were in store, initial TBT measurements without moving s_x^* were taken and analyzed ($\Delta s_x^* = 0$). Most s^* measurements were close to but not 0 ($\bar{s}_{x,meas}^* \approx .1m$) for most methods, where $\bar{s}_{x,meas}^*$ is the average s^* measurement. Therefore, relative measurements ($\bar{O}_{i+1} - \bar{O}_i$) between optics measurements when moving s^* will be considered as the expected beta beat, and star differences will no longer be zero. Relative measurements show the difference between average measurements and model in terms of trend.

The magnet strengths were then moved to $\Delta s_x^* = .1m$ according to the trim file corresponding to the appropriate Δs_x^* . After the movement, two TBT measurements were taken. The beam loss rate and beta around collimators are then monitored after every s_x^* movement and after every corrector kick to ensure most of the

beam is intact. The magnet strengths are also monitored to ensure correctness and confirm the movement has happened. This process was repeated afterward for $\Delta s_x^* = .3, .5\text{m}$ and again for backwards movement: $\Delta s_x^* = -.1, -.3, -.5\text{m}$.

After the appropriate TBT data had been gathered, the linear optics around IP were then measured through the curve-fitting method (CF) from RHIC and LR analysis. Upon observing the Δs^* measurements at IP8, both methods demonstrate on average the correct general trend of appropriate s^* movement, validating the methods mentioned in Section II. However, each method and modal decomposition technique show distinct results in terms of beta beat and s^* difference, relative beta beat and s^* difference, and error analysis.

A. Linear Regression vs Curve Fit

At each Δs^* movement, a comparison between β_x^* , s_x^* , β_y^* , s_y^* at IP8 measured by LR with DMD and CF is shown in Fig. 13, as well as the model from the sensitivity matrix.

The model curve (black) represents the expected value of the experimental measurement. The sensitivity matrix requests a transverse s^* change and outputs the currents and corresponding magnet strengths to be changed in the machine. The magnet strengths are fed into RHIC, and the blue and purple curve show the corresponding measurements of s^* from RHIC. To make this procedure consistent for the model, the current strengths are fed into MADX, and the black curve shows the corresponding "measurement" of s^* from MADX, demonstrating what the sensitivity matrix predicts for each of the linear optics.

For s_x^* , s_y^* , LR DMD establishes an average relative trend more close to the model than CF. Despite the small amount of measurements, LR DMD demonstrates a smaller "variance" (difference between two datasets at the same Δs_x^*) and a smaller overall beta beat and s^* difference from model between Δs^* measurements when compared to CFs'.

This is all quantitatively established in Table III. The second column compares the average variance between LR DMD and CF. These represent the consistency of the method. The third column compares the average difference between method used and the model; for β^* , this is the beta beat, for s^* , this is the difference between measurement and model. These represent the accuracy of the optics. The fourth column compares the average of the relative difference between each method used and the model. This represents the average relative movement compared to the model when ignoring accuracy, measuring the difference in trend between model and measurement.

Table III confirms that all three quantities are larger in CF than LR DMD in terms of s_x^* and s_y^* , demonstrating accurate results and consistency of the LR DMD method.

TABLE III. Average Variances, Average Differences and Average Relative Differences from Fig. 13. All measurements are in meters.

Method	Variance	Diff	Rel Diff
LR DMD β_x^*	0.15122	0.10956	0.06796
CF β_x^*	0.14877	0.22943	0.08628
LR DMD s_x^*	0.06849	0.05639	0.07500
CF s_x^*	0.65625	0.16199	0.19775
LR DMD β_y^*	0.02248	0.05389	0.02014
CF β_y^*	0.08457	0.05552	0.02969
LR DMD s_y^*	0.06278	0.064697	0.01176
CF s_y^*	0.22858	0.21173	0.25651

For β_x^* and β_y^* , the metrics between LR DMD and CF are similar in value. However, the average relative difference in β^* is larger for CF than for LR DMD, demonstrating a better beta beat measurement. This demonstrates that overall better accuracy, consistency, and relative trend that LR DMD has compared to CF.

B. Modal Decomposition Techniques

A comparison is also made between the modal decomposition techniques. Fig. 14 demonstrates measurements pertaining to varying turn interval and initial turn were included as well as exponential removal. This is more apparent when no modal decomposition method was used. This shows that removing the exponential is a valid preprocessing step in addition to the modal ones. It also shows the ambiguity of using different initial turns and intervals when measuring the beta function when no preprocessing is done.

When it comes to the modal methods, exponential removal seems to make little to their measurements. It can also be seen that without exponential removal or modal preprocessing, LR can be more or less accurate than CF at certain instances. This emphasizes that using some preprocessing such as exponential removal can enhance the quality of measurement. It also shows flexibility between using model-independent and dependent methods since when preprocessing is included, the linear optics measurements will be improved.

ICA does as well as DMD for s_x^* measurements, but fails with other optics such as at $\Delta s_x^* = .5$ for the s_y^* measurement as shown in Fig. 15, and with other optics measurements around the ring. This is due to the inconsistency of quality in the betatron modes when being distinguished as well as the low number of TBT data points taken for each Δs_x^* . If the betatron modes cannot be distinguished from the synchrotron and other modes, this will result in inadequately reconstructed BPM data and ultimately bad measurements. This demonstrates ICA to be less consistent in principle than DMD and even CF at certain optics, and may only be used if more data was taken.

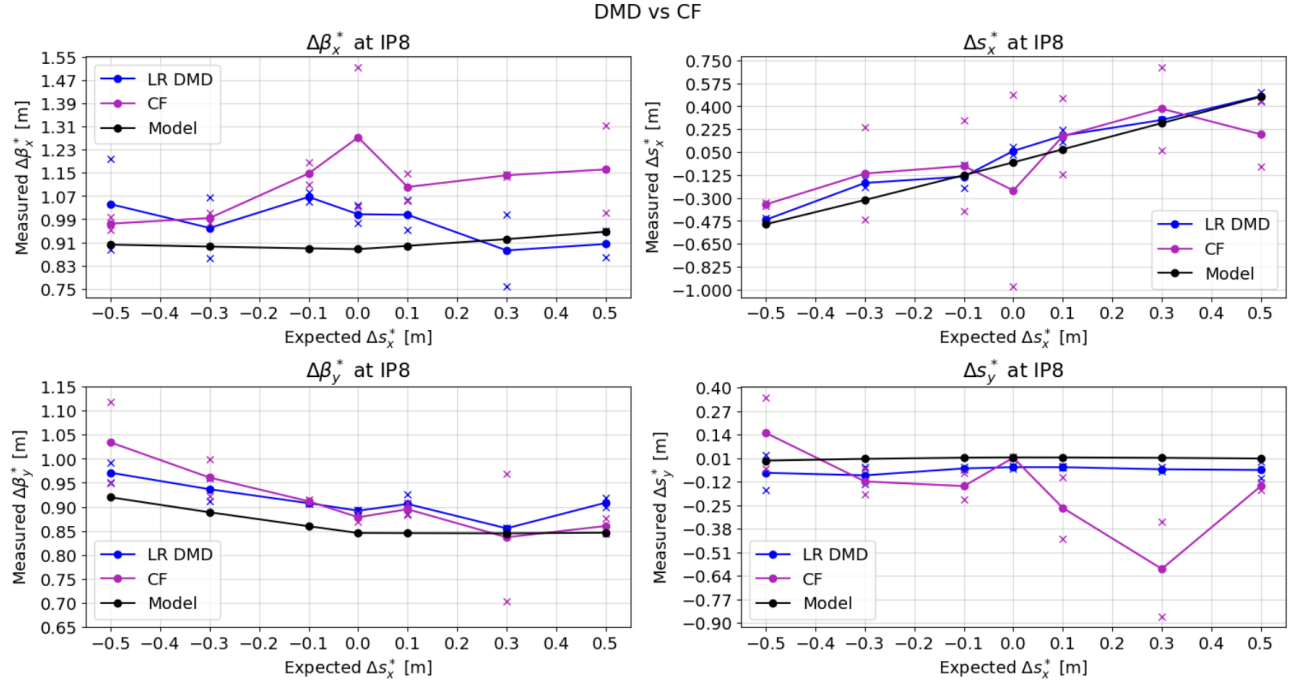


FIG. 13. Individual measurements marked with x's. The average between two measurements for each Δs_x^* movement is taken for resulting measurements in β_x^* , s_x^* , β_y^* , s_y^* at IP8 respectively. These lines are compared to the average CF measurements (magenta) and model (black).

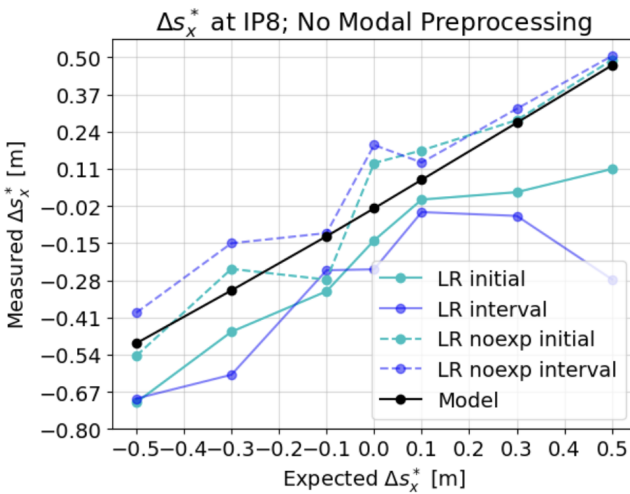


FIG. 14. The average between two measurements (not shown) for each Δs_x^* movement is taken for resulting LR measurements in s_x^* at IP8. Plain LR (Raw) is plotted with exponential removed (dashed) and not removed (solid) and with varying initial turn (cyan) and turn interval (blue). These are compared to the model (black).

PCA shows the most similarity to DMD. This is due to the similar nature of both methods; PCA and DMD both produce spacial modes using SVD techniques. The main difference is that PCA emphasizes orthogonality between modes while DMD emphasizes uncovering tem-

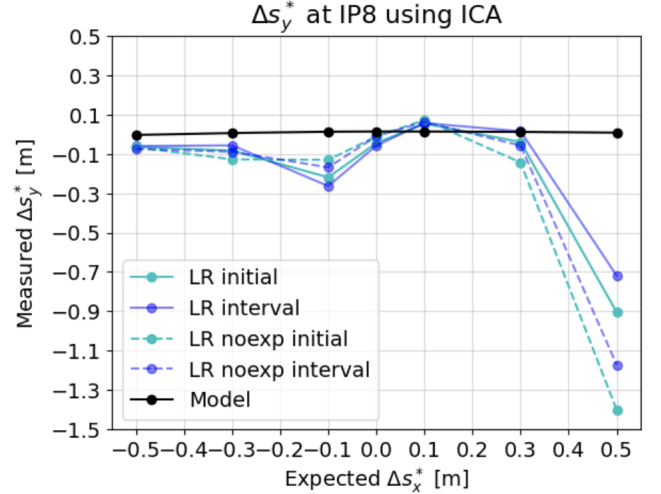


FIG. 15. The average between two measurements for each Δs_x^* movement is taken for resulting LR measurements in s_y^* at IP8. LR ICA method is plotted with exponential removed (dashed) and not removed (solid) and with varying initial turn (cyan) and turn interval (blue). These are compared to the model (black).

poral modes as well. In the case of RHIC TBT data, the spacial modes from DMD were close to orthogonal when uncovering temporal modes as well. This has its advantages, although by a smaller amount than raw data, when considering the spread between varying initial turn and

TABLE IV. Average of the spreads at each Δs_x^* between exponential removed and unremoved and varying initial and interval turn at IP8 from Fig. 16. All measurements are in meters.

Optics	PCA	DMD
β_x^*	0.00791	0.000448
s_x^*	0.00855	0.00193
β_y^*	0.00300	0.000176
s_y^*	0.0105	0.00111

interval which is more clearly shown in Fig. 16, as well as in Table IV.

Between these modal decomposition techniques, Fig 14–Fig 16 shows that PCA and DMD overall is the most accurate, consistent, and most correct trends for optics measurements when dealing with RHIC TBT data. It is shown that exponential removal and varying initial turn and interval overall doesn't make a difference between modal preprocessing results, demonstrating consistency. However, according to Table IV, DMD shows the least variation between exponential removal and varying initial and interval for s_x^* at IP8. This was also the case when looking at measurement results at other optics around the ring.

VI. CONCLUSION

The sensitivity matrix B was shown to consistently move the magnets such that s_x^* can be changed appropriately. All linear optics methods show an average general trend from $\Delta s_x^* = [-.5, .5]$ to move in the appropriate direction. This method can be extended to moving s^* in both transverse directions while taking care of the similar constraints as before.

Although all methods show low average beta beat throughout the ring as well as an average general trend when moving s_x^* , it was shown that DMD performs more consistently than ICA, and with less spread than ICA and PCA. From DMD, it is confirmed that Δs_x^* can be changed by the appropriate amount $\pm 5\text{cm}$. while keeping relative $\Delta\beta_x^* = \pm 10\%$ in a consistent manner. It was also shown that model-independent and dependent methods can both be used for optics measurements and further improved with decomposition techniques for comparison.

The usual curve fitting methods used to calculate the beta function at RHIC will implement DMD in the future as an optional feature. Other methods to measure linear optics at IP can also be looked at and compared to, such as the model dependent method of ICA, as cross-checking methods will produce the most accurate results for β^* and s^* . It was also shown that applying DMD to methods other than LR also improves the consistency and accuracy of the method.

This study is a preliminary one used to build confidence in s^* movement. In future experiments, Bayesian Optimization (BO) will be used to locate the optimal luminosity collision region within sPHENIX. Improving s^* movement will improve the accuracy of the s^* request from BO to RHIC. Other experiments may also apply these techniques to improve the accuracy and consistency of the movement of specific linear optics.

ACKNOWLEDGMENTS

This work is supported by DOE Office of Nuclear Physics under award number DE-SC0023518. This work is also supported by Brookhaven Science Associates, LLC under Contract No. DE-SC0012704 and DE-AC02-06CH11357 with the U.S. Department of Energy.

- [1] H. Werner and B. Muratori (CERN), Concept of luminosity, *Phys. Rev.* , 361 (2006).
- [2] P. Castro, *Luminosity and beta function measurement at the electron-positron collider ring LEP*, Ph.D. thesis, CERN (1996).
- [3] C. Liu, *Optics measurement and correction during beam acceleration in the Relativistic Heavy Ion Collider*, Tech. Rep. (BNL, Brookhaven National Lab.(BNL), Upton, NY (United States), 2014).
- [4] J. Safranek, Experimental determination of storage ring optics using orbit response measurements, *Nuclear Instruments and Methods in Physics Research Section A: Accelerators, Spectrometers, Detectors and Associated Equipment* , 27 (1997).
- [5] X. Huang, Linear optics and coupling correction with closed orbit modulation, *PHYSICAL REVIEW ACCELERATORS AND BEAMS* (2021).
- [6] R. E. Meller, *Decoherence of kicked beams*, Tech. Rep. (Fermilab, 1987).
- [7] S. C. for the sPHENIX Collaboration, sphenix: The next generation heavy ion detector at rhic, *Journal of Physics: Conf. Series* (2017).
- [8] M. G. Minty and F. Zimmermann, Transverse optics measurement and correction: Multiknobs, optics tuning, and monitoring, in *Measurement and control of charged particle beams* (Springer Nature, 2003) pp. 43–46.
- [9] X. Huang, Application of independent component analysis to fermilab booster, *Physical Review Special Topics—Accelerators and Beams* 8.6 (2005).
- [10] A. Hyvärinen and E. Oja, Independent component analysis: algorithms and applications, *Neural networks* 13.4–5 , 411 (2000).
- [11] J. H. Tu, Dynamic mode decomposition: Theory and applications, *J.Comput. Dyn.* 1 , 391 (2014).
- [12] B. W. B. et al, Extracting spatial-temporal coherent patterns in large-scale neural recordings using dynamic mode decomposition, *Journal of Neuroscience Methods* , 1 (2016).

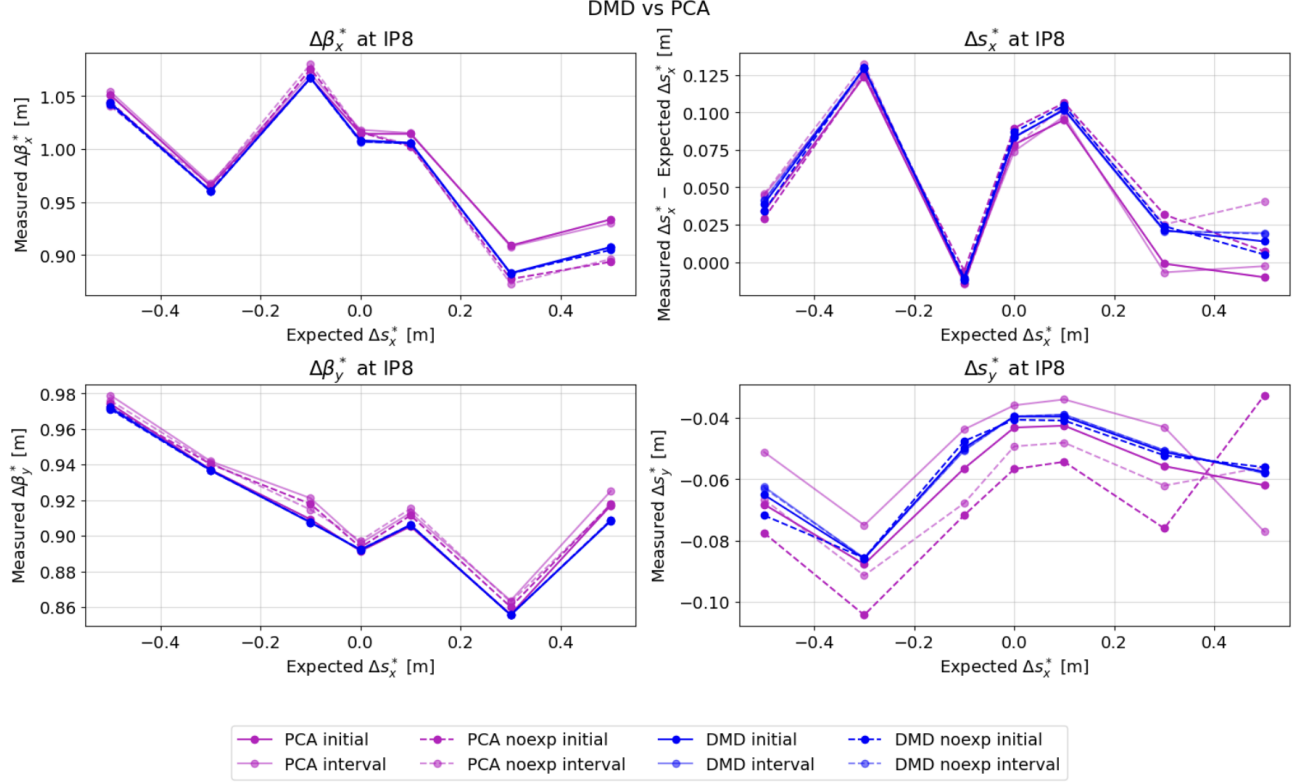


FIG. 16. The average between two measurements for each Δs_x^* movement is taken for resulting LR measurements in β_x^* , s_x^* , β_y^* , s_y^* at IP8. LR DMD and PCA method is plotted with exponential removed (dashed) and not removed (solid) and with varying initial turn (light) and turn interval (solid). For s_x^* , the Δs_x^* movements were subtracted out for clarity

- [13] N. Demo, Pydmd: Python dynamic mode decomposition, Journal of Open Source Software 3.22 , 530 (2018).
- [14] H. Wiedemann, *Particle accelerator physics*, 4th ed. (Springer Nature, 2015) pp. 213–231.
- [15] M. J. Syphers and R. Miyamoto, Direct measurements of beta-star in the tevatron, IEEE (2007).